First results of PRISMA satellite data applied to water quality monitoring in Argentina

Víctor Gauto
Instituto de Altos Estudios Espaciales Mario Gulich CONAE/UNC
Falda del Cañete, Argentina
victor.gauto@outlook.com

Anabella Ferral
Instituto de Altos Estudios Espaciales Mario Gulich CONAE/UNC
Falda del Cañete, Argentina
aferral@unc.edu.ar

Matias Bonansea
Instituto de Altos Estudios Espaciales Mario Gulich CONAE/UNC
Falda del Cañete, Argentina
mbonansea@ayv.unrc.edu.ar

Alejandro Farías
Grupo de Investigación Sobre Temas Ambientales y Químicos UTN-FRRe
Resistencia, Argentina
alefarias@ca.frre.utn.edu.ar

Marcelo Scavuzzo
Instituto de Altos Estudios Espaciales Mario Gulich CONAE/UNC
Falda del Cañete, Argentina
scavuzzo@conae.gov.ar

Osvaldo Cardozo
Instituto de Investigación Para el Desarrollo Territorial y del Hábitat Humano CONICET
Resistencia, Argentina
odcardozo@hum.unne.edu.ar

Alba German
Instituto de Altos Estudios Espaciales Mario Gulich CONAE/UNC
Falda del Cañete, Argentina
agerman@unc.edu.ar

Claudia Giardino
CNR-IREA
Milan, Italy
giardino.c@irea.cnr.it

***Abstract*—Water has historically been considered a renewable resource, however in the last century a sustained degradation of its quality has been observed, both in continental and oceanic systems due to anthropic impact. In this context, the management of water resources by satellite technology represents a central point in public policies since they allow anticipating and adapting to these disturbances. In this work, Sentinel 2-MSI multispectral and PRISMA hyperspectral sensors are used to carry out an analysis of different optical water types in North-East of Argentina. Convolutional procedure was used to compare sensors responses for atmospheric corrected products and RMSE (root mean square error), BIAS and MAE (mean absolute error) metrics were used to assess their performance. Differences below 1 percent were obtained in all cases, indicating an excellent match-up between both sensors. From hyperspectral PRISMA data it was possible to detect quantitative shift towards reddish wavelengths as turbidity of Parana River increases along a transect as well as an increase of the peak value in magnitude. This work opens new opportunities to monitor water quality changes related to optical constituents with deeper details in space and time in highly urbanized and perturbed regions.**

***Keywords*—PRISMA, Sentinel 2, hyperspectral, turbid waters, atmospheric correction, cromaticity, spectral signature**

I. Introduction

The study and monitoring of surface waters is essential for its conservation as a natural resource. The 2030 Agenda for Sustainable Development, by the United Nations [1], establishes to guarantee universal and equitable access to clean water, reduce the contamination of this resource and improve management and sanitation. A useful indicator is the proportion of healthy water bodies, that can be estimated by remote sensing techniques.

978-1-6654-8014-7/22/$31.00 ©2022 IEEE

Satellite remote sensing offers data from large areas, at regular times, systematically generating different processing level products. The parameters that are possible to estimate using this technology are concentration of total suspended solids, Secchi disk depth and chlorophyll-a concentration, among others [2]. Given the multidisciplinary characteristics of remote sensing, it is possible to couple it with machine learning techniques, showing positive results [3]. The combining of multiple existing satellite platforms can help to fill the information gap and improve the results accuracy [4]. Remote sensing is essential for understanding water bodies [5] and protect them.

By choosing the right sensor, it is possible to work with smaller water bodies, according to the spatial resolution. The constant data collection from Earth's surface allows the development of time series, which account for the evolution of a particular property over time. The use of different sensors, such as optical and radar, like Landsat-5, 7 and 8, and Sentinel-1 and 2 missions, have been useful for the spatio-temporal analysis of lakes properties [6]. The level of eutrophication in lagoons and its relationship with water quality has been studied through this approach [7] and its also allows to perform time series analysis in order to understand space-time changes [8], [9], offering more information to support decision making. The combination of space sensors allows the coupling of the data, extending the analysis period [10].

As it was mentioned before, biophysical parameters can be estimated from satellite information such as the concentration of chlorophyll-a for coastal waters [11] and continental water bodies [12]. In general, for lakes, lagoons, rivers and coastal areas constituted by type 1 waters [13], chlorophyll-a can be retrieved by remote sensing techniques easily than for type 2 waters [14]. The importance of knowing the concentration

of chlorophyll-a is that it allows to estimate the presence of algae and the eutrophication phenomenon. In this sense, water quality is usually monitored through these kind of biophysical parameters [15]. Turbidity is also used to follow water quality in wide rivers with high sediment contents, like Rio de la Plata in Argentina [16]. From turbidity measurements it is also possible to follow large-scale phenomena, such as droughts [17] and El Niño [18]. During the last years, hyperspectral sensors have also been used to estimate these variables [19].

Secchi disk deph is an important variable to estimate water transparency [20] and can be used to infer algal bloom occurrence in productive water bodies with very low sediments presence [21]. It can also be used to follow vertical mixing phenomena in shallow waters [14].

Landsat series, developed by NASA, and Sentinel-2 satellite constellation, by ESA within the framework of the Copernicus program, have proved its usefulness for estimating chlorophyll-a [9], [22], [23], Secchi disk depth [24], suspended solids [25] and water extent [26], [27]. Particularly, Sentinel-2 satellites have some of their bands in VIS-NIR region with 10 m of spatial resolution, 5 days of temporal resolution, free access to their image repository and high precision results [28] making them one of the most chosen data sets.

PRISMA (PRecursore IperSpettrale della Missione Applicativa, HyperSpectral Precursor of the Application Mission) is a pre-operative hyperspectral mission, by the Italian Space Agency (ASI) [29]. It was launched in March 2019 and their main objectives are qualify the technology, develop applications and provide products to scientific and institutional users. The main benefits are expected in the fields of forest analysis, precision agriculture, climate change, environmental research and water quality [30].

PRISMA offers atmospherically corrected surface reflectance products. When compared with Sentinel-2 products, the water quality estimated by PRISMA corresponds well with the expected results [31], [32]. In addition, other water characteristics such as phycocyanin concentration, can be obtained by PRISMA [33] images.

Freshwater ecosystems, such as lagoons, lakes, streams, rivers, wetlands, swamps, bogs, etc. are among the most threatened natural systems on the planet [34], mainly due changes in land use and climate variability. These shallow waters have represented a challenge for remote sensing due to their small size and high spatial complexity. The way to study them usually consists of deriving biophysical parameters from spectral data, requiring field measurements for validation. These are usually at specific sites, which cannot correctly represent properly the spatial variability of these dynamic systems; likewise, the logistics, costs and time associated with field work are limiting.

This is the case of Gran Resistencia Metropolitan Area (GRMA), Chaco province, North-East of Argentina, which is crossed by Negro river. Extensive rains, periods of drought and floods modify its route. The irregular river course across the plain generates meander lagoons [35], close to the population. Estimating the characteristics of these lentic water bodies is important to assess human activity impact in its water quality. In addition, this area is next to Paraná river, which is the second longest river in South America, with 4800 km. It begins at the confluence of the Rio Grande and Paranaíba rivers, in Brazil, and flows until Río de la Plata, Argentina, running eastern of the region of interest for this study. It is the main source of water for the GRMA, relevant for the fishing industry, tourism, as a cargo transport route for ships and recreational activities for nearby communities.

The research done in these area by remote sensing techniques is scarce or null. Some studies focus in land cover change [36] and the deforestation progress [37], but those focused on water bodies and rivers are not abundant. There are general studies at national level with remote sensing applications [9], [38], [39], but not specifically for GRMA. Research on the Paraná river usually covers the North basin, within the limits of Brazil; or the South basin, near Santa Fe city, Argentina, but without a water quality approach [40], [41].

The objective of this study is to characterize spectral responses of different surface water bodies by using hyperspectral satellite images acquired over small water bodies in GRMA and a transect in Parana river. Top of atmosphere and surface reflectance PRISMA spectral signatures were compared to Sentinel-2 equivalents. A convolution match-up was evaluated to properly compare both sensors.

II. Materials and Methods

A. Study Area

Fig. 1 shows the study region, GRMA, in the North-East of Argentina, in Chaco province, marked as a yellow star on the overview map.

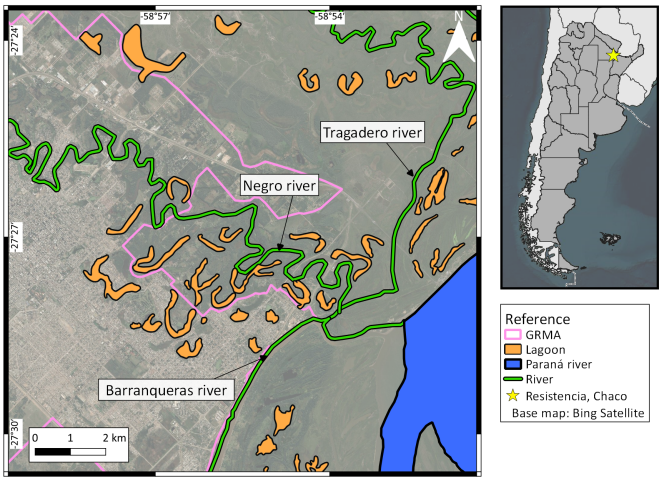

Fig. 1: Region of interest, mayor water bodies and rivers.

One of the main rivers in GRMA is Negro river, with a West-East direction. In the East, the Paraná's shore, and one of its branch, the Barranqueras river. The water bodies and rivers shown are constantly changing their size and distribution, due changes in Negro river flow, floods, drought, etc.

B. Satellite products

The PRISMA hyperspectral image was acquired on June 11, 2021. It has a spatial resolution of 30 m (panchromatic band at 5 m) and its VIS-NIR chanel has 63 spectral bands, 402-973 nm range. The swath is 30x30 km. Level 1 product is top of atmosphere reflectance (R_t), radiometrically corrected and calibrated, in radiance units (W/m^2-sr-μm).

The level 2D product is atmospherically corrected and geolocated, as surface reflectance (R_s, dimentionless). Users can access the catalog and acquire new images from the PRISMA website.

The atmospheric correction in PRISMA L2D considers two main parameters: aerosol optical thickness and water column, to correct the presence of atmospheric components, such as molecules and aerosol scattering and gas absorption. Radiative transfer equations are solved to minimize a cost funtion, between the radiance at top of atmosphere obtained by the models, and the radiance measured by the PRISMA sensor [42].

The Sentinel-2 multispectral image corresponds to June 10, 2021, acquired by the 2B platform, the day before the PRISMA satellite. The spatial resolution of the product depends on the spectral band, and can be 10/20/60 m. The swath is 110x110 km, 13 spectral bands, from 442-2185 nm, with different bandwidths. Processing level L1C corresponds to R_t product. Sentinel-2 R_s product is level L2A, atmospherically corrected.

The atmospheric correction of Sentinel-2 products is made by Sen2Cor processor [43]. Aerosols presence is corrected by the Dark Dense Vegetation algorithm [44]. Water vapor column effect is reversed by the Atmospheric Pre-corrected Differential Absorption algorithm [45].

This study is focused in the VNIR range, between 400-900 nm. Table I summarize the main characteristics of the used products.

TABLE I: PRISMA and Sentinel-2 main features.

Platform feature	Platform	
	PRISMA	***Sentinel-2***
Date	2021-06-11	2021-06-10
# of spectral bands	240	13
Spatial resolution (m)	30	10/20/60
Swath (km)	30	110
Spectral range (nm)	400-2505	442-2185

C. Sample points

The sample points, Fig. 2, are divided in two groups. For the study of different types of water, according to its spectral signature, seven sample points were selected, representing three different classes. To assess the change in the spectral signature across Paraná's river, points located in a transect were extracted from the hyperespectral product.

Types of water: The spectral signature analysis was made considering three types of water.

Type A water: Presents water bodies deep enough to appear black in the real color composite of the satellite products. This

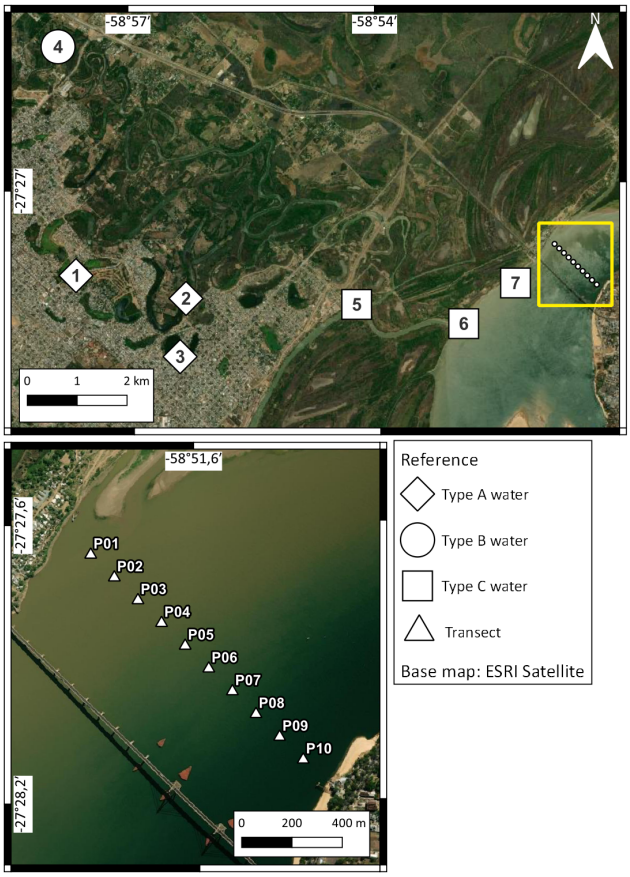

Fig. 2: Sample points in GRMA and transect in Paraná river.

is an indicator of low spectral response. Sites 1, 2 and 3 in Fig. 2 are located in ponds surrounded by urban areas.

Type B water: A single point (site 4 in Fig. 2) located in the center of a small (250 m) pond in La Ribera, North-West of the GRMA . Being within a populated area, its study is of interest to monitor its characteristics and how they change over time.

Type C water: Three representative lotic water sample sites were located, distributed on the West shore of Paraná river and one of its branches (sites 5, 6 and 7, Fig. 2), the Barranqueras river. Site 5 is of special interest, since it is the place from which the water treatment company of GRMA is supplied.

Due to the knowledge of the study area, the general characteristics of the types of water are: type A has high concentrations of chlorophyll-a (91.56 μg/L chlorophyll-a, 49.8 cm Secchi disk depth), due to a characteristic greenish color in the water body; type B has low sediment concentration, and usually does not present eutrophication problems, being considered clear water when compared to the other types; type C with high concentrations of suspended solids (29.00 mg/L total suspended matter, 69.25 NTU turbidity, < 1 μg/L chlorophyll-a), given the characteristics of the Paraná on the West coast. The parameter values were measured by GISTAQ (Research Group on Environmental and Chemical Issues), from UTN (National Technological University) in Resistencia.

Transect in Paraná River: A transect was drawn perpendicular to the direction flow of the Paraná river, with ten equidistant sample points, distanced by 130 m between each other, and the shores. Spectral signatures were extracted from the hyperspectral image, in order to evaluate the change in the reflectance of the water that passes from high sediment content (North-West coast) to clearer water (South-East coast).

Fig. 2 shows both sets of points over the study area. The upper image contains the distribution of the sample points for three water types. The yellow square at the right is detailed in the bottom image with ten sample points on the Paraná River transect.

D. Radiance to reflectance conversion, top of atmosphere

The PRISMA level 1 product (PRISMA L1), without atmospheric correction, presents the pixel values in radiance at top of atmosphere physical units (W/m^2-sr-μm). To properly compare with the equivalent Sentinel-2 L1C product, it must be converted to reflectance by applying the following equation:

$$R_{t,i} = \frac{L_i \cdot \pi}{E_{0,i} \cdot k \cdot cos(SZ)} \tag{1}$$

Where $R_{t,i}$ is top of atmosphere reflectance; L_i, PRISMA L1 radiance; $E_{0,i}$, the extraterrestrial solar spectra; k, dependent of the day of the year: $k = 1 + 0.0167 \cdot cos[2\pi \cdot (\text{Julian day} - 3)/365]^2$, 0.0167 is the Earth's orbit eccentricity; and SZ, the angle of incoming solar direction, solar zenith angle, given by PRISMA product metadata. Equation (1) is used for each spectral band i.

E. PRISMA and Sentinel-2 match-up

Surface reflectance (R_s) values given by PRISMA and Sentinel-2 are not directly comparable, due to differences in the spectral characteristics of the sensors. The spectral resolution for PRISMA is around 11 nm, for all VNIR bands. However, Sentinel-2 has bands with a bandwidth of 15 nm (B05 and B06) up to 106 nm (B08). Likewise, the center bands are not coincident in both sensors.

To perform a sensor-to-sensor comparison, it is convenient to simulate the Sentinel-2 values from PRISMA data using equation (2). This transformation allows the R_s obtained to be comparable. The reflectances calculated are the equivalents of what Sentinel-2 would measure with PRISMA sensor. A good correlation between simulated Sentinel-2 and PRISMA is an indicator of the quality of the measurement made by the hyperspectral sensor. If the differences between the spectral signatures of PRISMA L2D and simulated Sentinel-2 are small, it could be inferred a good quality in the data capture and correction from the hyperspectral sensor, since the MSI (MultiSpectral Instrument) sensor has low radiometric calibration uncertainty, producing reliable results [28]. The cross-sensor calibration required the spectral response functions (SRF) for MSI Sentinel-2.

$$\hat{R_s}(\lambda_i) = \frac{\int_k R_s(\lambda) \cdot SRF(\lambda) \cdot d\lambda}{\int_k SRF(\lambda) \cdot d\lambda} \tag{2}$$

$\hat{R_s}(\lambda_i)$ is the simulated reflectance from the multispectral sensor, for the bandwidth k, centered in λ_i. The hyperspectral reflectance is $R_s(\lambda)$. SRF(λ) is specific for the platform 2B of Sentinel-2 and spectral band λ. SRF for both platforms can be found in the Sentinel-2 mission website.

F. Performance metrics

To evaluate the closeness of the reflectance values for each wavelength, a series of performance metrics were selected. The R_s generated by the spectral convolution of Sentinel-2 L2A is taken as field truth. This transformation allows to combine the measurements of MSI sensor with the high spectral resolution of PRISMA. In the following equations, in all cases, the cross-sensor calibrated values were considered as *y*, and the values of PRISMA L2D as *x*, for *n* sampling points.

$$\text{RMSE} = \sqrt{\frac{\sum_{i=1}^{n} (y_i - x_i)^2}{n}} \tag{3}$$

$$\text{MAE} = \frac{\sum_{i=1}^{n} |y_i - x_i|}{n} \tag{4}$$

$$\text{SAM} = cos^{-1}\left(\frac{\sum_{i=1}^{n} y_i x_i}{\sqrt{\sum_{i=1}^{n} y_i^2}\sqrt{\sum_{i=1}^{n} x_i^2}}\right) \tag{5}$$

$$\text{BIAS} = \frac{\sum_{i=1}^{n} y_i - x_i}{n} \tag{6}$$

$$\text{R}^2 = 1 - \frac{\sum_{i=1} (x_i - y_i)^2}{\sum_{i=1} (x_i - \overline{x})^2} \tag{7}$$

RMSE, root mean square error (eq. 3), measures the precision between the compared data [46], sensitive to its distribution. MAE, mean absolute error (eq. 4), evaluates the precision without amplifying the deviations due extreme values [46]. SAM, spectral angle measure (eq. 5), considers spectral signatures as vectors in a *j*-dimensional space, where *j* is the number of spectral bands [47]. BIAS (eq. 6), measures the mean difference between both data sets, estimating the systematic error. R^2, Pearson's correlation coefficient squared (eq. 7), indicates a good data fitting the closer is to 1. RMSE, MAE and BIAS are in the same units as the evaluated parameter and SAM is in degrees.

These performance metrics are applied to find the deviations in the spectral signatures for the different types of water and to assess the closeness of PRISMA sensor signatures compared to Sentinel-2 MSI. A single metric is not enough, but its combination achieved a good interpretation of results.

III. Results and Discussion

A. Spectral signatures, surface reflectance

The spectral signatures from PRISMA level 2D (PRISMA L2D) and Sentinel-2 level L2A (S2 L2A) images are shown in Fig. 3. Values are in R_s, sharing the vertical axis. The wavelength range (λ), on the horizontal axis, was narrowed to match that of Sentinel-2 in the VNIR range, from 400 nm to 900 nm.

The dots in the Fig. 3 represents the individual values extracted from the different sample sites. The solid lines are the mean spectral signatures for each type of water.

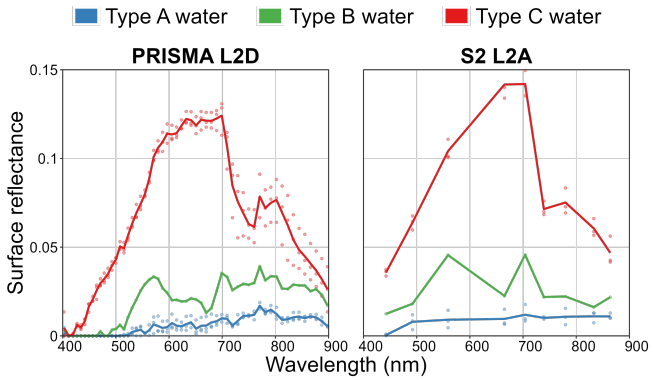

Fig. 3: Spectral signatures (surface reflectance R_s vs wavelenght λ) of three water types, per platform.

The spectral signatures given by PRISMA L2D shown a higher level of detail, in comparison with S2 L2A, taking advantage 63 bands in VNIR region.

Type A water, with a low spectral response and a slight increase along the wavelength, can be explained by the presence of sediments in the bottom of the water bodies [48], appearing black in the RGB composite image.

In both sensor type B water presents a peak around 570 nm, characteristic of chlorophyll-a and with low relative concentrations of suspended solids and CDOM [49]. Low values in the blue region (400-500 nm) and a peak at 550 nm correspond to the presence of chlorophyll-a in the water [50]. The absorption caused by chlorophyll-a is responsible for the low reflectances at 430 nm and 675 nm [51]. The peak seen at 700 nm is probably generated by the existence of phytoplankton, and the valley at 620 nm due to phycosianin [52].

Spectral signatures for type C water had the highest reflectance values. Possibly, the high suspended solids concentration is the cause of such values [49]. The curves present small deviations from each other, with minor differences between the shape of the curve and the reflectance values. The correspondence between the reflectances of PRISMA L2D and S2 L2A is evident at various wavelengths [32].

Comparing the spectral response for the same type water, in all cases, S2 L2A presents higher values than PRISMA L2D. The hiperspectral product, at short wavelengths, shows for type A and B water null values.

B. Match-up spectral signature

Fig. 4 shows the metrics values between the R_s extracted from S2 L2A product, compared with the simulated values applying equation 2, to obtain Sentinel-2 PRISMA-calibrated R_s.

The asterisks in the R^2 plot, in the Fig. 4, represent whether the given value of the linear correlation coefficient is significant at 95% confidence interval (p-value < 0.05). RMSE, BIAS and MAE where conveniently converted to percent. For

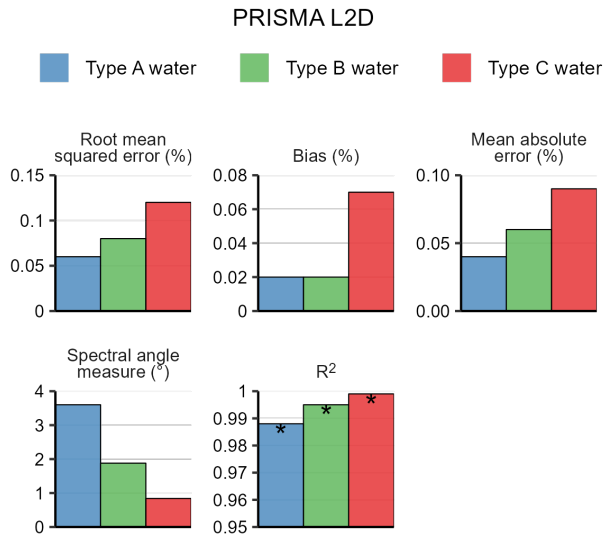

Fig. 4: Comparison between the spectral S2 match-up and PRISMA L2D product.

all water types, RMSE, BIAS, MAE present small values, none of those over 0.15% of deviation between datasets. The values of these metrics follow the same behaviour as seen in Fig. 3. Type C water, with the highest surface reflectances, presents the highest deviations, followed by type B and A water. However, the spectral signatures are the most similar in shape and values at type C water, with the lowest SAM and highest R^2.

Low values of RMSE, BIAS and MAE implied that PRISMA sensor has an equivalent spectral resolution as seen in MSI Sentinel-2 sensor. Similar results were obtained for water applications [32], showing the potential of PRISMA as a source of R_s to retrieve water quality products.

C. Spectral signatures, top of atmosphere

Fig. 5 shows the spectral signatures per type of water (in rows), for each sensor (in columns), and the comparison between bottom of atmosphere R_s (BOA, grey line) with automatic atmospheric correction; and top of atmosphere R_t (TOA, black line), non corrected atmospherically.

In all cases, TOA reflectances at short wavelengths presents high values. The different standard correction methods applied reduce this values, since both (PRISMA correction and Sentinel-2 Sen2Cor) measure the effect of the aerosols, that add more refletance due the dispersion of light cause by them.

The presence of aerosols at short wavelengths generates an increment in the signal captured by the sensor. The initial TOA reflectances, for all spectral signatures, were higher for Sentinel-2, mainly due to differences in the characteristics of the sensors of both platforms, as seen for the R_s products.

For type A and B water, the correction methods mostly reduced the reflectances values. For type C water, however, the atmospheric correction methods, for Sentinel-2 and PRISMA, increase some of the values, around the maximum at 600-

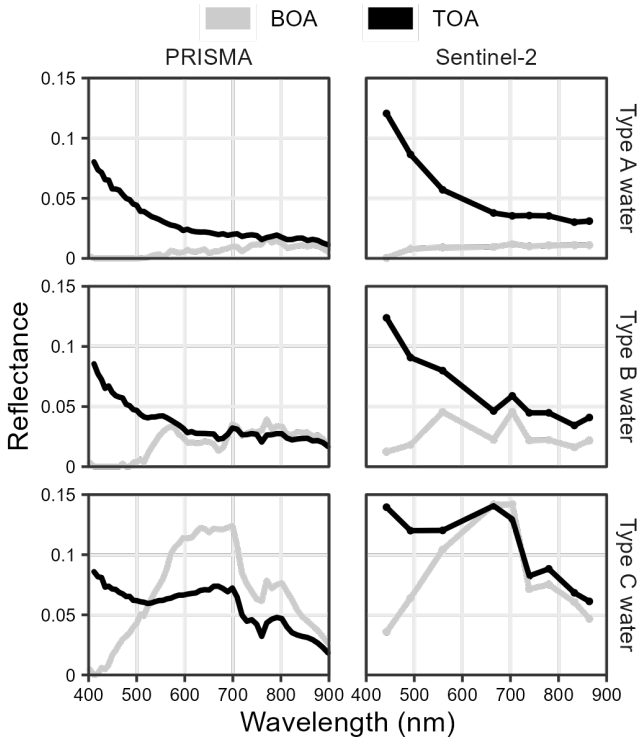

Fig. 5: Comparison between TOA and BOA reflectances, per type of water, per platform.

700 nm. The automated algorithms change the correction mechanisms in those water pixel where high signal is detected.

The difference in one day between the acquisition of the images, and the changes in the composition of the atmosphere, mainly optical thickness of aerosols and water vapor column, may be responsible for the differences in how Sen2Cor and PRISMA transform the data.

D. Paraná river transect

The spectral signatures of the transect sample points extracted from the PRISMA L2D product are plotted in Fig. 6. Ten spectral signatures are plotted, starting from P01, Paraná's North-West shore, up to P10, on the South-East, according to Fig. 2. The red circle in each plot indicates the maximum reflectance value of the spectral signature.

As the sample site moves from P01, with high sediment concentrations (turbidity 177 NTU), to P10, with clearer waters (turbidity 8.04 NTU), the shape of the water spectral response gradually changes, the maximum coordinates (R_s and λ) decrease. Turbidity values were estimated by Dogliotti's algorithm [53], present in ACOLITE software [54].

The spectral signature of the sample site P01 has the characteristics of type C water, due to its similarity in the spectral response (Fig. 3). The high reflectance values, around 700 nm, are indicative of a high suspended solids presence [49].

Site P10, in the opposite side, has a spectral signature that represents low concentrations of chlorophyll-a, suspended solids and CDOM [49]. Clear waters have a spectral behavior similar to the signature given by P10 [55].

The maximum coordinates at peak reflectance in each spectral signature of the Fig. 6 move from top to bottom, from right to left. That is, the waters associated with high concentrations of sediments have high reflectance values, at longer wavelengths. Clear waters have maximum reflectances with lower values and lower wavelengths.

IV. Conclusions and Future Work

Search, download, processing and visualization of a PRISMA hyperspectral images, at level 1 and 2D, corresponding to Gran Resistencia Metropolitan Area was achieved. Given the large number of spectral bands (63 in VNIR) it was

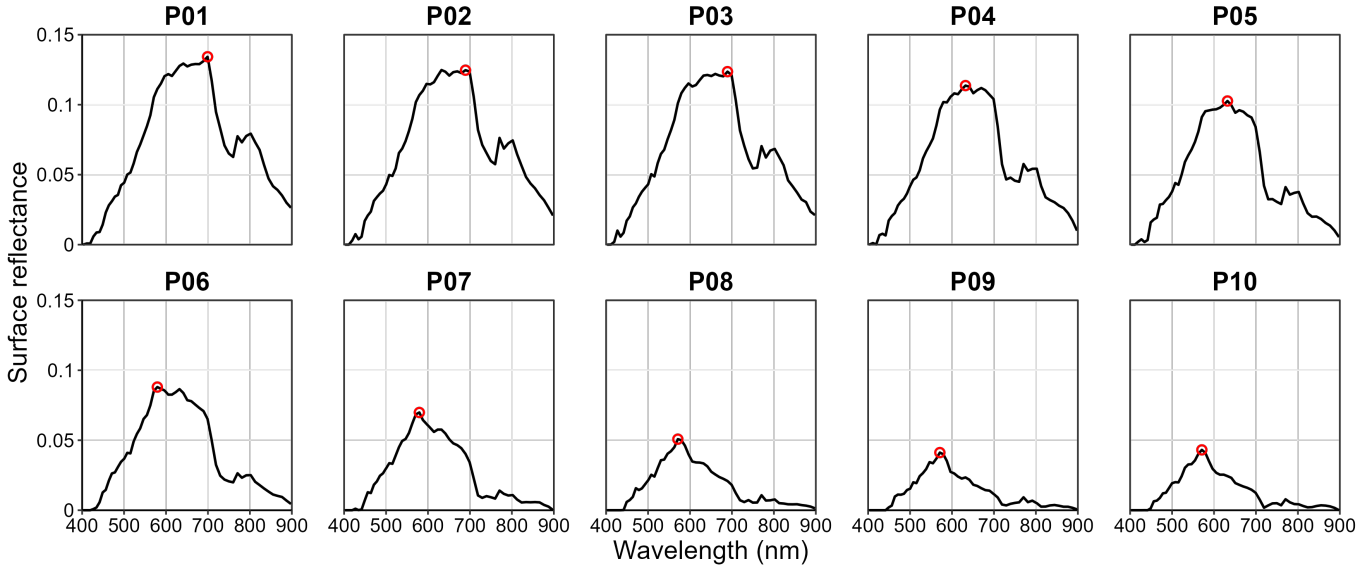

Fig. 6: Water spectral signature along the points located in Paraná river transect, using PRIMSA L2D.

possible to obtain detailed spectral signatures corresponding to three types of water present in the study region. The characteristics of the water could be differentiated thanks to the evaluation of the spectral response.

The spectral signatures given by PRISMA and Sentinel-2 were compared, at surface reflectance, and after a convolution calibration, the great similarity between sensors is evidenced. Since one of the objectives of the PRISMA mission is to test the technology, these results support the good quality of the products generated. The values of MAE, RMSE and BIAS between PRISMA 2D and S2-L2A are bellow 1% of deviation.

The hyperspectral study of ten points along a transect in Paraná River showed the change in the spectral response, from the region with the highest concentration of sediments (North-West side) to the one with the lowest concentration (South-East side).

Given the limited number of publications using PRISMA hyperspectral products in the study region, this study presents an advance in the spectral study of inland waters. In the future, it is expected to be able to extract even more information from the hundreds of spectral bands that PRISMA offers, to identify other pigments apart from chlorophyll-a. In addition, it will be possible to perform automatic classifications of coverage in the study area, model semi-empirical algorithms to generate maps that allow estimating variables, carry out comparisons with other sensors and validate the spectral response interpretations by field work and physicochemical laboratory analysis.

V. Acknowledgements

VG thanks the Master fellows from CONAE (National Commission for Space Activities, Argentina), research fellows from IREA (Institute for Electromagnetic Sensing of the Environment) in Milan, as part of CNR (National Research Council) of Italy and MAECI (Italian Ministry of Foreign Affairs and International Cooperation). This research is conducted in collaboration with the EC-H2020 EOXPOSURE project grant No 734541 and FONCyT-PICT -I-D-2018. PICT-2018-01447.

References

[1] U. Nations, "2030 agenda for sustainable development," vol. 11371, pp. 1–13, 2017.

[2] M. H. Gholizadeh, A. M. Melesse, and L. Reddi, "A comprehensive review on water quality parameters estimation using remote sensing techniques," *Sensors (Switzerland)*, vol. 16, 2016.

[3] F. S. Watanabe, G. T. Miyoshi, T. W. Rodrigues, N. M. Bernardo, L. H. Rotta, E. Alcântara, and N. N. Imai, "Inland water's trophic status classification based on machine learning and remote sensing data," *Remote Sensing Applications: Society and Environment*, vol. 19, 2020.

[4] V. Sagan, K. T. Peterson, M. Maimaitijiang, P. Sidike, J. Sloan, B. A. Greeling, S. Maalouf, and C. Adams, "Monitoring inland water quality using remote sensing: potential and limitations of spectral indices, bio-optical simulations, machine learning, and cloud computing," *Earth-Science Reviews*, vol. 205, p. 103187, 2020.

[5] I. Chawla, L. Karthikeyan, and A. K. Mishra, "A review of remote sensing applications for water security: Quantity, quality, and extremes," *Journal of Hydrology*, vol. 585, p. 124826, 2020.

[6] P. Huovinen, J. Ramírez, L. Caputo, and I. Gómez, "Mapping of spatial and temporal variation of water characteristics through satellite remote sensing in lake panguipulli, chile," *Science of the Total Environment*, vol. 679, pp. 196–208, 2019.

[7] D. Liu, H. Duan, S. Yu, M. Shen, and K. Xue, "Human-induced eutrophication dominates the bio-optical compositions of suspended particles in shallow lakes: Implications for remote sensing," *Science of the Total Environment*, vol. 667, pp. 112–123, 2019.

[8] H. C. Kim, S. Son, Y. H. Kim, J. S. Khim, J. Nam, W. K. Chang, J. H. Lee, C. H. Lee, and J. Ryu, "Remote sensing and water quality indicators in the korean west coast: Spatio-temporal structures of modis-derived chlorophyll-a and total suspended solids," *Marine Pollution Bulletin*, vol. 121, pp. 425–434, 2017.

[9] A. Germán, M. Shimoni, G. Beltramone, M. I. Rodríguez, J. Muchiut, M. Bonansea, C. M. Scavuzzo, and A. Ferral, "Space-time monitoring of water quality in an eutrophic reservoir using sentinel-2 data - a case study of san roque, argentina," 11 2021.

[10] F. Gohin, D. V. der Zande, G. Tilstone, M. A. Eleveld, A. Lefebvre, F. Andrieux-Loyer, A. N. Blauw, P. Bryère, D. Devreker, P. Garnesson, T. H. Fariñas, Y. Lamaury, L. Lampert, H. Lavigne, F. Menet-Nedelec, S. Pardo, and B. Saulquin, "Twenty years of satellite and in situ observations of surface chlorophyll-a from the northern bay of biscay to the eastern english channel. is the water quality improving?," *Remote Sensing of Environment*, vol. 233, p. 111343, 2019.

[11] J. He, Y. Chen, J. Wu, D. A. Stow, and G. Christakos, "Space-time chlorophyll-a retrieval in optically complex waters that accounts for remote sensing and modeling uncertainties and improves remote estimation accuracy," *Water Research*, vol. 171, p. 115403, 2020.

[12] L. Rodríguez-López, I. Duran-Llacer, L. González-Rodríguez, R. A. del Rio, R. Cárdenas, O. Parra, R. Martínez-Retureta, and R. Urrutia, "Spectral analysis using landsat images to monitor the chlorophyll-a concentration in lake laja in chile," *Ecological Informatics*, vol. 60, 2020.

[13] A. Morel and L. Prieur, "Analysis of variations in ocean color," *Limnology and Oceanography*, vol. 22, pp. 709–722, 7 1977.

[14] D. Liu, H. Duan, S. Loiselle, C. Hu, G. Zhang, J. Li, H. Yang, J. R. Thompson, Z. Cao, M. Shen, R. Ma, M. Zhang, and W. Han, "Observations of water transparency in china's lakes from space," *International Journal of Applied Earth Observation and Geoinformation*, vol. 92, p. 102187, 2020.

[15] K. T. Peterson, V. Sagan, P. Sidike, A. L. Cox, and M. Martinez, "Suspended sediment concentration estimation from landsat imagery along the lower missouri and middle mississippi rivers using an extreme learning machine," *Remote Sensing*, vol. 10, 2018.

[16] F. P. Maciel, P. E. Santoro, and F. Pedocchi, "Spatio-temporal dynamics of the río de la plata turbidity front; combining remote sensing with in-situ measurements and numerical modeling," *Continental Shelf Research*, vol. 213, p. 104301, 1 2021.

[17] V. S. Martins, A. Kaleita, C. C. Barbosa, A. C. Fassoni-Andrade, F. de Lucia Lobo, and E. M. Novo, "Remote sensing of large reservoir in the drought years: Implications on surface water change and turbidity variability of sobradinho reservoir (northeast brazil)," *Remote Sensing Applications: Society and Environment*, vol. 13, pp. 275–288, 2019.

[18] D. A. Romero-Rodríguez, L. A. Soto-Mardones, J. Cepeda-Morales, J. P. Rivera-Caicedo, and E. A. Inda-Díaz, "Satellite-derived turbidity in front of small rivers mouths in the eastern tropical pacific coast of mexico," *Advances in Space Research*, vol. 66, pp. 2349–2364, 2020.

[19] V. Garg, A. S. Kumar, S. P. Aggarwal, V. Kumar, P. R. Dhote, P. K. Thakur, B. R. Nikam, R. S. Sambare, A. Siddiqui, P. R. Muduli, and G. Rastogi, "Spectral similarity approach for mapping turbidity of an inland waterbody," *Journal of Hydrology*, vol. 550, pp. 527–537, 2017.

[20] F. M. Breunig, W. P. Filho, L. S. Galvão, F. Wachholz, and M. A. G. Cardoso, "Dynamics of limnological parameters in reservoirs: A case study in south brazil using remote sensing and meteorological data," *Science of the Total Environment*, vol. 574, pp. 253–263, 2017.

[21] E. M. Isenstein, D. Kim, and M. H. Park, "Modeling for multi-temporal cyanobacterial bloom dominance and distributions using landsat imagery," *Ecological Informatics*, vol. 59, p. 101119, 2020.

[22] A. G. Alarcón, A. Germán, A. Aleksinkó, M. F. G. Ferreyra, C. M. Scavuzzo, and A. Ferral, "Spatial algal bloom characterization by landsat 8-oli and field data analysis," *International Geoscience and Remote Sensing Symposium (IGARSS)*, vol. 2018-July, pp. 9292–9295, 2018.

[23] X. Sòria-Perpinyà, E. Vicente, P. Urrego, M. Pereira-Sandoval, A. Ruíz-Verdú, J. Delegido, J. M. Soria, and J. Moreno, "Remote sensing of cyanobacterial blooms in a hypertrophic lagoon (albufera of valència, eastern iberian peninsula) using multitemporal sentinel-2 images," *Science of the Total Environment*, vol. 698, p. 134305, 2020.

[24] M. Bonansea, M. Ledesma, R. Bazán, A. Ferral, A. German, P. O'Mill, C. Rodriguez, and L. Pinotti, "Evaluating the feasibility of using sentinel-2 imagery for water clarity assessment in a reservoir," *Journal of South American Earth Sciences*, vol. 95, p. 102265, 2019.

[25] I. Caballero, F. Steinmetz, and G. Navarro, "Evaluation of the first year of operational sentinel-2a data for retrieval of suspended solids in medium- to high-turbiditywaters," *Remote Sensing*, vol. 10, 2018.

[26] A. Ferral, E. Luccini, A. Aleksinkó, and C. M. Scavuzzo, "Flooded-area satellite monitoring within a ramsar wetland nature reserve in argentina," *Remote Sensing Applications: Society and Environment*, vol. 15, p. 100230, 2019.

[27] U. Bhangale, S. More, T. Shaikh, S. Patil, and N. More, "Analysis of surface water resources using sentinel-2 imagery," *Procedia Computer Science*, vol. 171, pp. 2645–2654, 2020.

[28] D. Phiri, M. Simwanda, S. Salekin, V. R. Nyirenda, Y. Murayama, and M. Ranagalage, "Sentinel-2 data for land cover/use mapping: A review," 7 2020.

[29] M. Meini, A. Bini, L. Giunti, E. Fossati, and R. Formaro, "Hyperspectral payload for italian prisma programme," *Optical Payloads for Space Missions*, pp. 183–213, 2015.

[30] R. Loizzo, R. Guarini, F. Longo, T. Scopa, R. Formaro, C. Facchinetti, and G. Varacalli, "Prisma: The italian hyperspectral mission," vol. 2018-July, pp. 175–178, IEEE, 2018.

[31] C. Giardino, M. Bresciani, F. Braga, A. Fabbretto, N. Ghirardi, M. Pepe, M. Gianinetto, R. Colombo, S. Cogliati, S. Ghebrehiwot, M. Laanen, S. Peters, T. Schroeder, J. A. Concha, and V. E. Brando, "First evaluation of prisma level 1 data for water applications," *Sensors*, vol. 20, p. 4553, 8 2020.

[32] M. Niroumand-Jadidi, F. Bovolo, and L. Bruzzone, "Water quality retrieval from prisma hyperspectral images: First experience in a turbid lake and comparison with sentinel-2," *Remote Sensing*, vol. 12, pp. 1–21, 2020.

[33] R. E. O'Shea, N. Pahlevan, B. Smith, M. Bresciani, T. Egerton, C. Giardino, L. Li, T. Moore, A. Ruiz-Verdu, S. Ruberg, S. G. Simis, R. Stumpf, and D. Vaičiūtė, "Advancing cyanobacteria biomass estimation from hyperspectral observations: Demonstrations with hico and prisma imagery," *Remote Sensing of Environment*, vol. 266, 2021.

[34] E. L. Hestir, V. E. Brando, M. Bresciani, C. Giardino, E. Matta, P. Villa, and A. G. Dekker, "Measuring freshwater aquatic ecosystems: The need for a hyperspectral global mapping satellite mission," *Remote Sensing of Environment*, vol. 167, pp. 181–195, 2015.

[35] S. A. P. de Neiff, C. A. Patiño, J. J. Neiff, and A. O. Ramos, "Water quality in the lower section of the negro river (chaco, argentina)," *FACENA*, vol. 19, pp. 67–85, 2003.

[36] M. L. Clark, T. M. Aide, H. R. Grau, and G. Riner, "A scalable approach to mapping annual land cover at 250 m using modis time series data: A case study in the dry chaco ecoregion of south america," *Remote Sensing of Environment*, vol. 114, pp. 2816–2832, 2010.

[37] M. Baumann, C. Levers, L. Macchi, H. Bluhm, B. Waske, N. I. Gasparri, and T. Kuemmerle, "Mapping continuous fields of tree and shrub cover across the gran chaco using landsat 8 and sentinel-1 data," *Remote Sensing of Environment*, vol. 216, pp. 201–211, 2018.

[38] A. Ferral, E. Luccini, V. Solis, A. Frery, A. Aleksinko, I. Bernasconi, and C. M. Scavuzzo, "In-situ and satellite monitoring of water quality of an eutrophic lake with an artificial air diffusion system," *IEEE Latin America Transactions*, vol. 16, pp. 627–633, 2018.

[39] E. M. Silveira, V. C. Radeloff, S. Martinuzzi, G. J. M. Pastur, L. O. Rivera, N. Politi, L. Lizarraga, L. S. Farwell, P. R. Elsen, and A. M. Pidgeon, "Spatio-temporal remotely sensed indices identify hotspots of biodiversity conservation concern," *Remote Sensing of Environment*, vol. 258, p. 112368, 2021.

[40] M. Salvia, F. Grings, H. Karszenbaum, P. Ferrazzoli, P. Kandus, A. Soldano, and L. Guerriero, "Monitoring inundation dynamics in paranà river, argentina, by c and l band sar," *International Geoscience and Remote Sensing Symposium (IGARSS)*, vol. 1, pp. 102–105, 2008.

[41] Z. Y. Marchetti, E. M. Latrubesse, M. S. Pereira, and C. G. Ramonell, "Vegetation and its relationship with geomorphologic units in the parana river floodplain, argentina," *Journal of South American Earth Sciences*, vol. 46, pp. 122–136, 2013.

[42] *PRISMA Products Specification Document*. Italian Space Agency, 2020.

[43] M. Main-Knorn, B. Pflug, J. Louis, V. Debaecker, U. Müller-Wilm, and F. Gascon, "Sen2cor for sentinel-2," p. 3, SPIE, 10 2017.

[44] Y. J. Kaufman and C. Sendra, "Algorithm for automatic atmospheric corrections to visible and near-ir satellite imagery," *International Journal of Remote Sensing*, vol. 9, pp. 1357–1381, 1988.

[45] D. Schläpfer, C. C. Borel, J. Keller, and K. I. Itten, "Atmospheric precorrected differential absorption technique to retrieve columnar water vapor," *Remote Sensing of Environment*, vol. 65, pp. 353–366, 1998.

[46] B. N. Seegers, R. P. Stumpf, B. A. Schaeffer, K. A. Loftin, and P. J. Werdell, "Performance metrics for the assessment of satellite data products: an ocean color case study," *Optics Express*, vol. 26, p. 7404, 2018.

[47] F. A. Kruse, A. B. Lefkoff, J. W. Boardman, K. B. Heidebrecht, A. T. Shapiro, P. J. Barloon, and A. F. Goetz, "The spectral image processing system (sips)-interactive visualization and analysis of imaging spectrometer data," *Remote Sensing of Environment*, vol. 44, pp. 145–163, 1993.

[48] A. Albert and C. Mobley, "An analytical model for subsurface irradiance and remote sensing reflectance in deep and shallow case-2 waters," *Optics Express*, vol. 11, p. 2873, 2003.

[49] E. F. F. da Silva, E. M. L. de Moraes Novo, F. de Lucia Lobo, C. C. F. Barbosa, M. A. Noernberg, L. H. da Silva Rotta, C. T. Cairo, D. A. Maciel, and R. F. Júnior, "Optical water types found in brazilian waters," *Limnology*, vol. 22, pp. 57–68, 1 2021.

[50] G. Dall'Olmo and A. A. Gitelson, "Effect of bio-optical parameter variability on the remote estimation of chlorophyll-a concentration in turbid productive waters: Experimental results (applied optics (2005) 44 (412-422))," *Applied Optics*, vol. 44, p. 3342, 2005.

[51] A. Morel and A. Bricaud, "Theoretical results concerning light absorption in a discrete medium, and application to specific absorption of phytoplankton," *Deep Sea Research Part A. Oceanographic Research Papers*, vol. 28, pp. 1375–1393, 11 1981.

[52] D. R. Mishra, I. Ogashawara, and A. A. Gitelson, *Bio-optical Modeling and Remote Sensing of Inland Waters*. Elsevier, 2017.

[53] A. I. Dogliotti, K. G. Ruddick, B. Nechad, D. Doxaran, and E. Knaeps, "A single algorithm to retrieve turbidity from remotely-sensed data in all coastal and estuarine waters," *Remote Sensing of Environment*, vol. 156, pp. 157–168, 2015.

[54] RBINS, "ACOLITE User Manual," 2021.

[55] V. P. Curtarelli, E. F. F. da Silva, F. de Lucia Lobo, C. C. F. Barbosa, and E. M. L. de Moraes Novo, "Water transparency in a brazilian reservoir," *Proceedings of the XIX Brazilian Symposium on Remote Sensing*, pp. 3287–3290, 2019.